出國報告(出國類別：參加國際研討會)

參加第35屆電機電子工程師學會醫學暨生物工程社群年度國際研討會報告

The 35th Annual International Conference of the IEEE Engineering in Medicine and Biology Society

服務機關: 國立中正大學電機工程學系

姓名職稱: 余松年教授

派赴國家: 日本

出國期間: 民國102 年7 月3 日至102 年7 月8 日

報告日期: 民國 102 年 7 月 16 日

國立中正大學『前瞻製造系統頂尖研究中心』

補助出席國際會議報告

Advanced Institute of Manufacturing with High-Tech Innovations, National Chung Cheng University

Subsidizing Attending International Academic Conferences Report

（請於 回國後一個月內繳交 Please submit it one month after beneficiary's return within the same accounting year）

<table>
<tr><td colspan="2">補助者姓名：余松年
Beneficiary's Name: Sung-Nien Yu</td><td colspan="2">單位、職稱：電機工程學系/教授
Title and Dept.: Electrical Engineering/ Professor</td></tr>
<tr><td colspan="2">會議時間 Date：
2013 年(yyyy) 07 月(mm) 03 日(dd)至 to
2013 年(yyyy) 07 月(mm) 07 日(dd)</td><td>地點(國、州、城市)
Location(Country, State, City)</td><td>日本、大阪
Japan, Osaka</td></tr>
<tr><td rowspan="2">會議正式名稱
Conference Name</td><td colspan="3">中文 Chinese：第 35 屆電機電子工程師學會醫學暨生物工程社群年度國際研討會</td></tr>
<tr><td colspan="3">英文 English：The 35th Annual International Conference of the IEEE Engineering in Medicine and Biology Society</td></tr>
<tr><td rowspan="2">發表之論文題目
Title of the paper presented</td><td colspan="3">中文 Chinese：(共 3 篇) (1)一個使用智慧型手機的可攜式即時心電圖辨識系統；(2) 以型態學特徵偵測心肌缺血事件的技術探討; (3) 一個為研究主動感知所研發的觸覺替代視覺系統 (皆為通訊作者)</td></tr>
<tr><td colspan="3">英文 English：(3 papers) (1) A Portable Real-time ECG Recognition System Based on Smartphone; (2) Detection of Myocardial Ischemia Episode Using Morphological Features; (3) A Tactile Vision Substitution System for the Study of Active Sensing (Serve as the corresponding author)</td></tr>
</table>

摘要

今年適逢國際電子電機工程學會(Institute of Electrical and Electronics Engineers, IEEE)醫學和生物工程社群(Engineering in Medicine and Biology Society)的國際年度會議於日本大阪舉行，本研討會為生物醫學工程研究領域中極重要的會議，每年會議均獲得世界各國專家學者的重視和熱烈參與，會議論文並收錄於電機領域中最重要的 IEEE IEL 西文資料庫。很幸運地，今年度本人和所指導的研究生共有三篇論文被大會接受，分別為 (1) A Tactile Vision Substitution System for the Study of Active Sensing（一個為研究主動感知所研發的觸覺替代視覺系統）; (2) A Portable Real-time ECG Recognition System Based on Smartphone（一個使用智慧型手機的可攜式即時心電圖辨識系統）; (3) Detection of Myocardial Ischemia Episode Using Morphological Features（以型態學特徵偵測心肌缺血事件的技術探討），且皆被排訂為口頭報告(Oral Presentation)，實在是莫大的榮耀。感謝前瞻製造系統頂尖研究中心的補助，使得本人和學生們得以成行，並有機會指導學生在大型的國際會議中進行演說，將研究室近年來的研究心血以及台灣的研究能量與世界分享。

目次

一、目的

參與生物醫學工程領域的大型國際學術會議，將研究室近年來的研究心血，以及台灣的研究能量與世界分享；並與國際生物醫學工程領域的學者專家交流，同時指導研究所學生在大型的國際會議中用英語演講並進行討論。

二、參加活動過程

本次研討會舉辦時間為7/3~7/7，前面剛好遇到本人接到國科會的簽呈於6/29~7/3赴以色列出席台以雙邊第二期共同研究計畫成果發表會及會後交流訪問，因此於7/2下午在以色列耶路薩冷大學發表完共同研究計畫成果之後，即向同行的副主委及其他學者告別，搭乘半夜的飛機，由以色列台拉維夫機場出發，經韓國首爾，趕赴日本大阪與學生會合，一起參加研討會。

行程表如表一所示。

表一 參加研討會行程表

日期	行程	地點
7/2~7/3	由以色列台拉維夫出發，經韓國首爾，前往日本大阪（由以色列台拉維夫飛韓國首爾段機票費不列入本案經費補助申請）	以色列台拉維夫 > 韓國首爾 > 日本大阪
7/4	參加第35屆電機電子工程師學會醫學暨生物工程社群年度國際研討會	日本大阪
7/5	參加第35屆電機電子工程師學會醫學暨生物工程社群年度國際研討會；上午研究生許伯恩於8:00~9:30的9.2.1 Vision and Eye Sensing場次專題演講	日本大阪
7/6	參加第35屆電機電子工程師學會醫學暨生物工程社群年度國際研討會	日本大阪
7/7	參加第35屆電機電子工程師學會醫學暨生物工程社群年度國際研討會；上午研究生顏子豪於11:00~12:30的10.4.2 mHealth I場次專題演講；下午研究生范振翔於13:30~15:00的1.4.7 Biomedical Signal Classification through ECG Analysis場次專題演講	日本大阪
7/8	由日本大阪返回台北	日本大阪 > 台北

本人於 7/2 搭乘大韓航空 KE0958 班機於晚間 23:00 出發，於韓國時間 7/3 的15:10抵達韓國首爾的仁川國際機場，經過轉機檢查，於 19:15 搭乘大韓航空 KE0721 班機離開韓國，於日本時間 7/3 的 20:55 抵達日本大阪關西機場，於機場和三位研究生會合，搭乘 JR 線快速電車前往會議地點：大阪國際會議中心附近的旅館。

7/4 一早即率同學生們一同前往大阪國際會議中心，先完成報到並領取會議相關資料，即開始聆聽相關的研討會。中午有大會主席的歡迎演說，並邀請哈佛大學的John Halamka（約翰・哈拉姆卡）進行專題演講，是有關生物醫學工程技術如何聯繫技術提供者、購買者和病人的需要之間的探討，由生物醫學工程研究的歷史回顧講到各國的相關技術發展近況探討，深入剖析，令我受益良多。下午和學生們分別聆聽研討會及與海報展示部分的學者交流。晚上19:30出席大會所舉辦的歡迎晚宴，遇到許多來至台灣和世界各地的學者，許多台灣的學者平常並不容易碰面，都是在國際研討中碰到面並交流。

7/5 上午，本人的研究生許伯恩於8:00~9:30的9.2.1 Vision and Eye Sensing （視覺與眼的感測)場次安排有專題演講，題目是：A Tactile Vision Substitution System for the Study of Active Sensing（一個為研究主動感知所研發的觸覺替代視覺系統）。本研究起源於本人和以色列的魏茲曼科學院共同提出的台灣-以色列雙邊合作計畫「城市環境中之感官替代研究」，演講中介紹本雙邊合作計畫的主要研究成果，是一個提供給盲人使用的主動式觸覺替代視覺系統。我們針對這樣系統開發了兩個演算法，分別是影像轉換和影像追跡演算法。影像轉換演算將所獲得高解析度的影像降取樣、透過特徵提取及二值化，以有效地轉換成低解析度的觸覺刺激訊號，使得物件的特徵更能夠辨識。影像追跡系統則是精確地提供相機位置，幫助研究人員分析使用者的主動式感覺行為，以回饋修正系統。希望本研究的成果能夠提供盲人使用主動式觸覺替代視覺的方式，更容易偵測到周圍的環境，增進生活的便利性和安全感。

因為演講排在最早的場次，因此 7/5 一早即督促學生們早早用餐，趕赴8:00就開始的專題演講場合。演講期間，與會聽眾和研究人員提出許多建設性的問題，有非常密切的互動討論，會後並交換聯絡方式。其他時間，帶領學生分頭聆聽其他場次的口頭演講以及瀏覽壁報展示，指導他們觀摩別人的演說方式，並與各國的研究人員充分討論互動。

7/6 到會場聆聽口頭演講以及瀏覽壁報展示，與參展的國外學者交換意見，請教了許多問題，並交換名片。特別是遇到好幾位台灣來的研究人員，平時在台灣並不容易碰面，反而是在國際研討會中經常見面，其中包含交通大學、長庚大學、義守大學、中原大學的教授、工研院的資深工程師以及目前在美國矽谷工作的工程師，在現場與他們親切互動，除了介紹學生們相關領域的先進們和工業界的研究人員之外，更交換彼此在不同學校、不同領域的研究經驗和心得，交流研究的經驗，並交換名片，並討論未來合作的可能。

7/7 上午，本人的研究生顏子豪於11:00~12:30的10.4.2 mHealth I（行動健康 I）場次安排有專題演講，題目是：A Portable Real-time ECG Recognition System Based on Smartphone（一個使用智慧型手機的可攜式即時心電圖辨識系統），本研究目的在於建立一套基於智慧型手機的即時心搏辨識輔助診斷系統，傳統心電圖機只能觀測特定時間之心臟電氣活動，瞬間發生的心律不整不一定能被完整記錄。因此，本實驗室開發可攜式即時辨識系統渴望成為上述問題之解決方法。本系統主要是在智慧型手機的Android平台上實現無線藍芽心電圖的感測與處理系統，系統可分為訊號擷取、R 點偵測、特徵擷取、類神經網路分類及辨識結果呈現。測試訊號使用被廣泛認定之MIT-BIH資料庫，搭配輸出入裝置首先將數位資料轉成即時的類比方式輸出，然後利用低功率的單晶片對心電圖訊號做類比/數位轉換，之後透過藍芽晶片與手機做資料傳輸，智慧型手機能即時收到數位心電圖訊號。在R點偵測方面，首先使用帶通濾波器移除雜訊對訊號的干擾，接著採用改良過的即時R點偵測演算法找到R點，取出64 點的QRS區段後，再使用高階統計特徵以描述五階小波轉換後之特定次頻帶，共計算27個高階統計特徵，再搭配3個RR間隔的頻域相關特徵。接著驗證類神經網路效能，並選出最佳樣本比例分配之權重，然後將此演算法移植到智慧型手機上。結果顯示本系統可以高達98.34%的辨識率分辨七種心電圖訊號，而且手機上實際辨識一個心搏只需0.078秒，每5秒更新一次分析資訊，顯示本研究演算法的高效能及即時系統的可行性。

7/7 下午研究生范振翔於13:30~15:00的1.4.7 Biomedical Signal Classification through ECG Analysis（透過心電圖分析的生醫訊號分類)場次安排有專題演講,題目是:Detection

of Myocardial Ischemia Episode Using Morphological Features（以型態學特徵偵測心肌缺血事件的技術探討）。在本研究中，我們提出使用形態特徵辨識心肌缺血的心搏和正常心搏。在一般情況下，心肌缺血導致心電圖中的變化，如ST段的下降。當下降到一定的電壓，此心搏會被判定為心肌缺血心搏。為了強調在心電圖中ST段的變化，將QRS波形以直線取代，再由小波分解至階層五，此階層經過測試為最能反應ST段變化的階層，接著再擷取12個形態學特徵。當使用支持向量機為分類器，並使用交叉驗正進行系統效能的評估，可以達到敏感性（Sensitivity）、特異性（Specificity）和準確性（Accuracy）分別為95.20％，93.29％，和93.63％的高分辨效能，與近年來的相關文獻比較，系統效能卓越。

接連的口頭的演講報告，除了前幾天利用晚上時間幫同學們預演之外，當天並在現場幫他們打氣，必要時協助他們回答現場的問題。現場主席和聽眾們提出許多問題，反應非常熱烈。晚餐，一起赴大阪市區聚餐，並慶祝參與會議的成功和收穫。晚上即收拾行李準備回台灣。

7/8 上午一早，退房之後即趕赴大阪關西機場。因為當初赴以色列時，國科會安排全部人員搭乘大韓航空。當考慮由以色列趕赴日本大阪及回台灣的行程時，和旅行社討論之後，考慮行程的連貫、方便性和經濟性（最便宜），因此回程仍搭乘大韓航空，唯一的缺點是必須到韓國首爾轉機。中午 12:10 搭上大韓航空 KE0724 由日本大阪出發，於韓國時間 7/8 的 14:00抵達韓國首爾的仁川國際機場，經過轉機檢查，於 16:20 搭乘大韓航空 KE0693 班機離開韓國，於台灣時間 7/8 的 17:50 抵達台灣桃園國際機場，搭乘 高鐵和計程車回嘉義中正大學的宿舍。

三、心得

“Annual International Conference of the IEEE Engineering in Medicine and Biology Society”（電機電子工程師學會醫學暨生物工程社群年度國際研討會），是電機電子工程領域最大的國際組織：電子電機工程學會(Institute of Electrical and Electronics Engineers, IEEE)的醫學和生物工程社群(Engineering in Medicine and Biology Society)所舉辦的年度國際大型會議，是生物醫學工程研究領域中極重要的會議，每年會議均獲得世界各國專

家學者的重視和熱烈參與，會議論文並收錄於電機領域中最重要的IEEE IEL 西文資料庫。今年適逢本年度會議（第35屆）於日本大阪舉行，有超過2600篇論文投稿。

今年大會非常用心，特別邀請到十四位大師級人物當作重點主題講員（Keynote Speakers），於開幕以及每天的排定時段中進行專題演講，探討生物醫學工程中不同次領域的最新發展，並與現場各國來賓進行直接的交流。這十四位重點主題講員分別是：

(1) John Halamka, U.S.A.（約翰哈・拉姆卡，美國）;

(2) Shinya Yamanaka, Japan（山中伸彌，日本）;

(3) Yoonchae Cheong, Korea（蔡莊尹，韓國）;

(4) Hiroaki Kitano, Japan（北野宏明，日本）;

(5) Pablo Laguna, Spain（巴勃羅・拉古納，西班牙）;

(6) Yoshinobu Sato, Japan（佐藤慶喜，日本）;

(7) Sandro Carrara, Switzerland（桑德羅・卡拉拉，瑞士）;

(8) Peter Hunter, New Zealand（彼得・亨特，紐西蘭）;

(9) Natalia Trayanova, U.S.A.（納塔利婭・措雅諾娃，美國）;

(10) Theodore W. Berger, U.S.A.（西奧多・W・伯傑，美國）;

(11) Mitsuo Kawato, Japan（川人光男，日本）;

(12) Catherine Mohr, U.S.A（凱瑟琳・莫爾，美國）;

(13) Yuan-Ting Zhang, Hong Kong（張袁婷，香港）;

(14) Nicos Maglaveras, Greece（尼科斯・馬革拉維拉斯，希臘）.

本次會議分為十二個大主題（Theme），以下各分多個小主題（Track），分口頭及壁報方式發表，內容非常多樣而充實。本次會議的十二個大主題整理如下：

Theme 1: Biomedical Signal Processing（主題一：生醫訊號處理）

Theme 2: Biomedical Image and Image Processing（主題二：生醫影像與影像處理）

Theme 3: Bioinstrumentation: Sensors, Micro, Nano and Wearable Technologies（主題三：生醫儀器：感測器，微奈米與穿戴式技術）

Theme 4: Bioinformatics and Computational Biology; Systems Biology, Modeling

Methodologies（主題四：生物資訊與計算生物學；系統生物學，建模方法）

Theme 5: Cardiovascular and Respiratory Systems Engineering（主題五：心臟血管與呼吸系統工程）

Theme 6: Neural Engineering, Neuromuscular Systems & Rehabilitation Engineering(主題六：神經工程，神經肌肉系統與復健工程）

Theme 7: Molecular and Cellular Biomechanics, Tissue Engineering, Biomaterials（主題七：分子與細胞生物力學，組織工程，生物材料）

Theme 8: Bio-Robotics, Surgical Planning and Biomechanics（主題八：生物機器人，手術規劃與生物力學）

Theme 9: Therapeutic & Diagnostic Systems, Devices and Technologies, Clinical Engineering（主題九：治療與診斷系統，儀器與技術，臨床工程）

Theme 10: Healthcare Information Systems, Telemedicine（主題十：健康照護資訊系統，遠距醫療）

Theme 11: Biomedical Engineering Education and Society（主題十一：生物醫學工程教育與社群）

Theme 12: Healthcare Technologies in Major Disasters（主題十二：主要災害的健康照護科技）

今年適逢本年度會議（第35屆）於日本大阪舉行，有超過2600篇論文投稿，很幸運地，本人和所指導的研究生共有三篇論文被大會接受，分別為 (1) A Tactile Vision Substitution System for the Study of Active Sensing（一個為研究主動感知所研發的觸覺替代視覺系統）; (2) A Portable Real-time ECG Recognition System Based on Smartphone（一個使用智慧型手機的可攜式即時心電圖辨識系統）; (3) Detection of Myocardial Ischemia Episode Using Morphological Features（以型態學特徵偵測心肌缺血事件的技術探討），且皆被排訂為口頭報告(Oral Presentation)，實在是莫大的榮耀。第一篇論文安排在7/5上午8:00~9:30的9.2.1 Vision and Eye Sensing（視覺與眼的感測）場次發表，第二篇和第三論文分別安排在7/7的上午11:00~12:30的10.4.2 mHealth I（行動健康 I）和下午13:30~15:00的1.4.7 Biomedical Signal Classification through ECG Analysis(透過心電圖分析的生醫訊號分類）場次發表。由本人與研究生共同發表並回答參與者的提問，反應非常踴躍，從與

其他研究人員的直接討論之中獲得許多寶貴的經驗和啟發。會議期間遇到許多由國內及其他國家來的先進們,在現場與各國的專家直接面對面就相關議題進行討論,受益良多，同時也建立了許多難得的友誼。

此次會議，本人帶許伯恩、顏子豪、范振翔三位研究生同行，除了指導他們以英語演講及溝通的方法和技巧，並引薦他們認識國內外生物醫學工程領域的專家，他們皆表示受益良多。此行除了參加國際性的學術會議之外，也藉由現場的醫療儀器展示瞭解最新的臨床及研究型醫療儀器發展趨勢，並也利用每天會後的空檔參觀日本大阪的歷史古蹟、經濟活動及人文風景，深刻體會當地的文化氛圍，收穫良多。

感謝前瞻製造系統頂尖研究中心的補助，使得本人和學生們得以成行，並有機會指導學生在大型的國際會議中進行演說，將研究室近年來的研究心血，以及台灣的研究能量與世界分享。

四、建議事項

有鑑於本次會議的成功經驗，敦請國科會多補助國內學者及研究生類似的大型國際學術會議，使得國內的研究人員，特別是研究所學生，有機會與各國專家互動交流，除了吸取國際研究的經驗之外，能最直接地向他們介紹台灣的研究成果，使台灣的研究能推向國際，與國際接軌。

五、攜回資料名稱及內容

1. The 35th Annual International Conference of the IEEE Engineering in Medicine and Biology Society（第35屆電機電子工程師學會醫學暨生物工程社群年度國際研討會）Program Book（會議議程）一本

2. Quick Guide & Addendum（會議快速指引與附錄）一本

3. 會議論文光碟一片

六、附錄一（具代表性之活動照片）

圖一：本人於會場入口

圖二：開幕典禮

圖三：本人與研究生們；左起：許伯恩、范振翔、顏子豪、本人

圖四：研究生許伯恩發表演說場景

圖五：研究生顏子豪發表演說場景

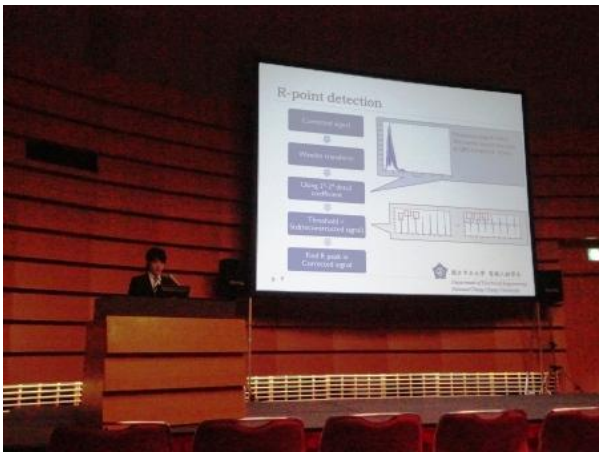

圖六：研究生范振翔發表演說場景

圖七：會場巧遇本人讀博士班時的同實驗室老師和研究伙伴；左起：Durand 教授的友人、Durand 教授的學生 Sahin 博士、Durand 教授、本人

圖八：會場巧遇義守大學的張國清教授（左一）

圖九：會場的海報展示區熱烈討論狀況

圖十：會場的生物醫學研究儀器展示一隅

七、附錄二（所發表論文）

A Tactile Vision Substitution System for the Study of Active Sensing*

Brian Hsu, Cheng-Han Hsieh, Sung-Nien Yu, Ehud Ahissar, Amos Arieli, and Yael Zilbershtain-Kra

***Abstract*—This paper presents a tactile vision substitution system (TVSS) for the study of active sensing. Two algorithms, namely image processing and trajectory tracking, were developed to enhance the capability of conventional TVSS. Image processing techniques were applied to reduce the artifacts and extract important features from the active camera and effectively converted the information into tactile stimuli with much lower resolution. A fixed camera was used to record the movement of the active camera. A trajectory tracking algorithm was developed to analyze the active sensing strategy of the TVSS users to explore the environment. The image processing subsystem showed advantageous improvement in extracting object's features for superior recognition. The trajectory tracking subsystem, on the other hand, enabled accurately locating the portion of the scene pointed by the active camera and providing profound information for the study of active sensing strategy applied by TVSS users.**

I. INTRODUCTION

The visually impaired people usually need to struggle in their daily lives to explore their outside environment. If more information of the environment can be provided in some way with the assistance of recent technology, then they could adapt to the environment more rapidly, via build-in natural learning processes [1, 2].

Sensory substitution for the visually impaired was first introduced by Bach-y-Rita and coworkers [3-5]. They invented the first sensory substitution system, which is a chair that allow blind to "see" via tactile actuators attached to their back and activated by a video camera. Later versions used other body parts with the latest version including actuator matrix placed on blind's tongue. The information was captured by the camera and fed back to the tactile device. This device is known as a tactile vision substitution system (TVSS) which offers people who suffer from lacking sight an opportunity to make a change.

A TVSS translates visual input, usually from a video camera, into the output of a tactile stimulation array. With the assistance of digital image processing techniques, the most significant features of the image could be extracted and provided as augmented sensation to the visually impaired. As a sequel, the users could more accurately distinguish foreground objects from the background.

Since the idea of sensory substitution was introduced, researchers gradually recognized the importance of actively moving the camera in the use of the TVSS. Because tactile resolution in the fingers is far more limited than the visual resolution (and so is the resolution of the arrays of tactile actuators relative to the number of camera pixels), the user of TVSS usually need to move the camera around to try to identify an object. This process is termed "active sensing." [6] The knowledge about how people develop effective strategies to actively sense the environment is also an important issue in the development of a TVSS.

(a) (b) (c)

Figure 1. TVSS system setup. (a) VTMouse ; (b) VTMouse with the active camera and pointer; (c) active sensing experiment.

This study stem from a cooperation project about sensory substitution between the Laboratory for the Study of Adaptive Perceptual Processing directed by Prof. Ehud Ahissar and the Active Sensing Laboratory directed by Dr. Amos Arieli at the Weizmann Institute of Science in Israel and the Biomedical Signal Processing and System Design Laboratory directed by Prof. Sung-Nien Yu at the National Chung Cheng University in Taiwan. The Israeli team set up experiments for active sensing with a TVSS while the Taiwanese team developed image processing algorithms aiming to enhance active sensing performance of the experiments. A trajectory tracking algorithm was jointly developed to understand participants' active sensing strategies.

This system contains two parts, namely (1) image processing and (2) trajectory tracking. The image processing part converts the color images acquired from the camera into lower resolution binary images with valuable features reserved, which designated to generate adequate output for the tactile device. The trajectory tracking part, on the other hand, tracks the trajectory of the participant on the stimuli and provides information for the study of active sensing strategies to explore the environment, without vision, using only TVSS.

II. SYSTEM OVERVIEW

The TVSS contains a tactile stimulation device and a camera. Tactile stimuli was provided by the VTMouse (Tactile World, Ra'anana, Israel) , as shown in Fig. 1 (a). The VTMouse is a standard size computer mouse for the blind [7], which consists three tactile stimulation arrays of 32 pins each (4x8) and provide tactile stimuli to the fingers at different heights (4 levels).

*Research supported by the National Science Council and the Ministry of Education, Taiwan, Republic of China and the Ministry of Science and Technology, Israel.

Brian Hsu, Cheng-Han Hsieh, and Sung-Nien Yu are with the Department of Electrical Engineering and the Advanced Institute of Manufacturing with High-tech Innovations, National Chung Cheng University, Chiayi County, Taiwan (corresponding author's phone: +886-5-2720411 ext 33205; fax: +886-5-2720862; e-mail: ieesny@ccu.edu.tw).

Ehud Ahissar, Amos Arieli, and Yael Zilbershtain-Kra are with the Department of Neurobiology, Weizmann Institute of Science, Rehovot, Israel (e-mail: ehud.ahissar@weizmann.ac.il; Amos.Arieli@weizmann.ac.il; yaelzilb@gmail.com).

A miniature video camera (active camera) (VQ25B-P37P; Filtech Corp., Yangchon-Gu Seoul, Korea) was attached to the VTMouse, as depicted in Fig. 1 (b) as the visual input sensor. In parallel to the miniature camera is a red laser pointer (605nm) which provides a marker associated with the location of the VTMouse. A wide view camera (fixed camera; 1280x1024, RGB, 15Hz) was arranged in a fixed location (Fig. 1 (C) to the left of the participant). With this arrangement, the movement of the active camera is identifiable in the fixed wide image taken by the fixed camera for further analysis.

III. IMAGE PROCESSING ALGORITHM FOR THE TVSS

Figure 2 shows the block diagram of the imaging processing algorithms developed for the TVSS. The color video frames acquired by the CCD camera, originally represented with red, green, and blue (RGB) attributes, were first transferred into hue, intensity, and saturation (HIS) color space [8]. Only the intensity part of the frame was reserved and represented as the grey-levels of the image. Image enhancement with histogram equalization [8] followed to make the foreground objects more separable form the background. The enhanced image needed to be further processed with downsampling, low-pass filtering, thresholding, and morphological process in order to generate suitable output for the tactile stimulation array. These methods are explained separately as follows.

A. Discrete Wavelet Transform for Downsampling

The tactile stimulation array had only 96 (12x8) pins as output. Compared to the image frame with a size of 640x480, the tactile array was far less in size. Therefore, the array could only display a very small part of an image, or, alternatively, the image could be shrunk to smaller resolution, a process termed downsampling. In our previous works [7-9], we have demonstrated the high capability of discrete wavelet transform (DWT) in downsampling an image into a quarter of the original size while preserving the most important features. Therefore, we also applied DWT as a downsampling processor in the study.

Figure 3 (a) shows the procedure of a two-dimensional DWT. With low-pass (*h[n]*), high-pass (*g[n]*) filters, and down-sampling operator (↓2), each row of the input image *x[n]* is firstly separated into the low-frequency (L) and high-frequency (H) parts. The similar column operators proceed to separate each column into low-frequency (L) and high-frequency (H) parts. In this manner, the image is separated into four subbands, namely LL, LH, HL, and HH, with different frequency attributes, as depicted in Fig. 3 (b).

After two dimensional DWT, an image is divided into four subband components of the same size (Fig. 2(b)). The high-frequency bands contain rapidly changing information such as noises and edges. The low-frequency bands, on the other hand, contain the features with low variety such as the shape of an object. The LL part was reserved as the downsampled version of the original image [8]. Moreover, since the property of the low-pass and high-pass filters used in the DWT is determined by the mother wavelet, the mother wavelet Rbio6.8 was empirically chosen to reserve the most image power after downsampling.

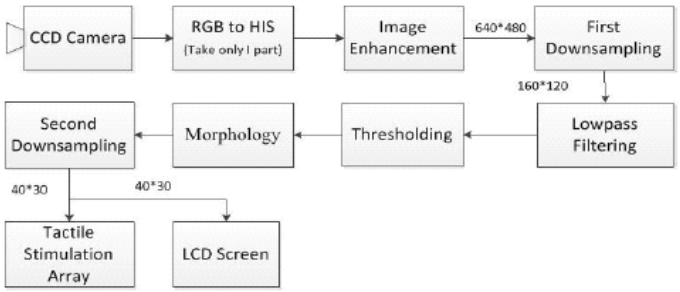

Figure 2. Diagram of the image processors for the TVSS.

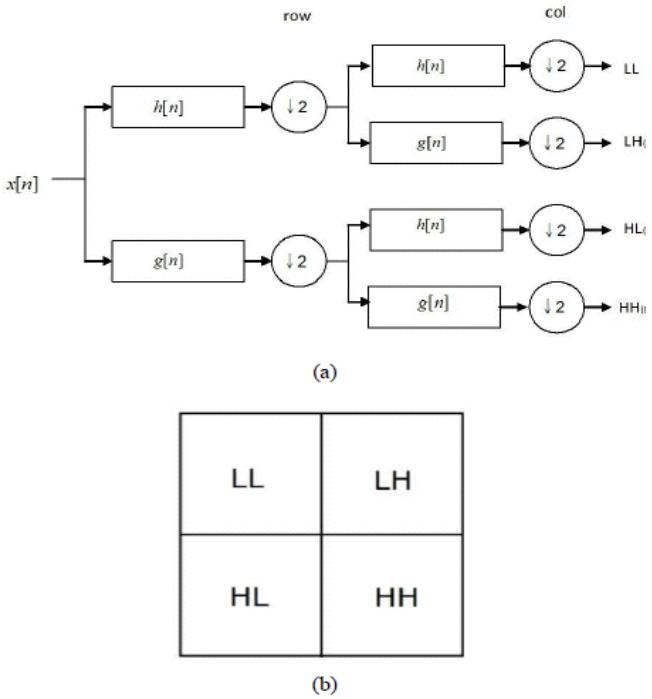

Figure 3. Two-dimensional discrete wavelet transform (DWT). (a) concept of 2D DWT; (b) different subband components after 2D DWT.

Two downsampling processes were used in the study. The first downsampler was used to reduce the size of original image such that the computational load of the following process was reduced. The second downsampler was applied after all the image processing had been done and then further reduced the image into a size of 40x30 to better fit the dimension of the tactile device.

B. Low-pass Filtering and Thresholding

A 5x5 mask average filter [6] was used as the low-pass filter to eliminate noise and smooth abnormal edges in the image. A thresholding operator followed to convert a grayscale image into a binary image. The threshold value was empirically determined to be 0.6 which resulted in the best performance.

C. Morphology Methods

After down-sampling, low-pass filtering, and thresholding, the acquired color image was transformed into a down-sampled binary image. However, shape defects and

missing areas of objects were to be fixed. Morphology methods [10], including dilation and erosion, were employed to tackle this problem.

Dilation is the process to gradually enlarge the boundaries of regions of foreground pixels. The function is expressed as

$$D = B \oplus S = \{x | (\hat{S})_x \cap B\} \quad (1)$$

where B represents structuring elements of dilation operator and S represents the image which is to be dilated. With this operator, the areas of foreground pixels grow in size and holes within those regions become smaller.

Erosion is the inverse of dilation. It erodes away the boundaries of regions of foreground pixels. The function is expressed as

$$E = B \ominus S = \{x | (S)_x \subseteq B\} \quad (2)$$

where B represents structuring elements of erosion operator and S represents the image which is to be eroded. With this method, areas of foreground pixels shrink in size and holes within those areas become larger.

The dilation operator was first applied to connect broken lines and holes inside objects. The erosion operator followed to erode the boundary regions back to the original size. With these operators, holes inside the image were filled.

IV. TRAJECTORY TRACKING ALGORITHM

A. *Diagram of the Trajectory Tracking Algorithm*

Figure 4 is the block diagram of the trajectory tracking procedure. Before tracking, the acquired images from the two cameras were downsampled to reduce the computational load of the following process. The laser pointer was used for identifying the location of the participant on the wide view image. Since the laser light may sometimes scatter and cause errors in tracking, we firstly identify the location of the red spot recorded by the fixed camera based on the difference image of the present and previous frames. The location was considered the probable center of the images acquired by the active camera. We then searched for the real center in the vicinity of the location for the most similar image region acquired by the fixed camera compared to the active camera image using the maximal index calculated from the crosscorrelation function [8]. As a result, the strategy used by the participants could be analyzed through tracking the trajectory of the participants on the stimuli during active sensing tasks [12].

B. *Correlation Coefficient as a Similarity Measure*

In trajectory tracking, we had to measure the similarity between the active camera image and image blocks of the fixed camera image. Pearson correlation coefficient [6], which measures the linear correlation of two variables, was chosen as a similarity measure. The correlation coefficient index is defined as

$$r = \frac{\sum_m \sum_n (A_{mn} - \bar{A})(B_{mn} - \bar{B})}{\sqrt{(\sum_m \sum_n (A_{mn} - \bar{A})^2)(\sum_m \sum_n (B_{mn} - \bar{B})^2)}} \quad (3)$$

where variables **A** and **B** are two different arrays, m and n are the indexes of the array elements in the row and the column, respectively, and $\bar{A}$ and $\bar{B}$ are the means of **A** and **B**, respectively. The value of the correlation coefficient index r is between -1 and 1. The higher the r value is the more similar **A** and **B** are.

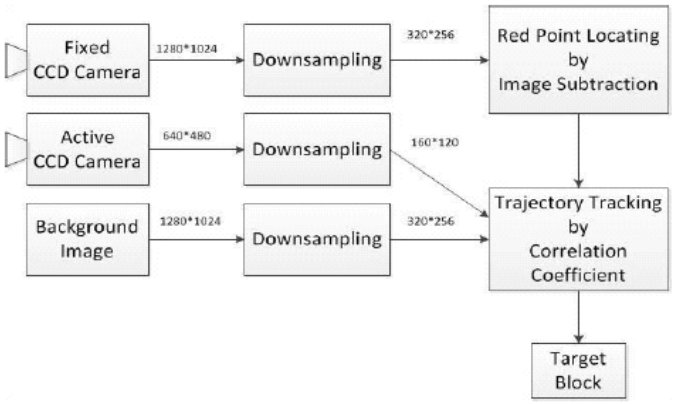

Figure 4. Diagram of trajectory tracking.

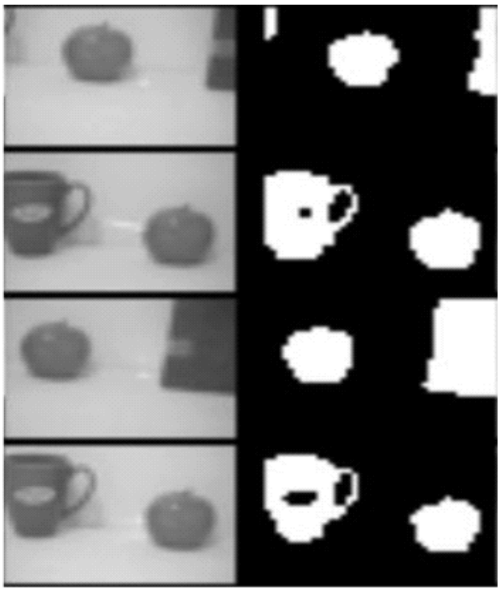

Figure 5. Result of the TVSS image processing algorithm; left column: downsampled grayscale image; right column: binary image after processing.

V. EXPERIMENTAL RESULTS AND DISCUSSIONS

To test the performance of the system, active sensing experiments were conducted in the laboratory at Weizmann Institute of Science in Israel. The participants were eye masked and asked to identify the objects placed in front of a blank white wall. The responses of the participants were recorded by the active camera for analysis.

Figure 5 shows one result of the image processing algorithm for the proposed TVSS. The left column shows the downsampled grayscale image frames. The second column shows the binary images after processing, which are fed into the tactile device as input. Three objects, namely a cup, an apple, and a book, were observed in the recorded sequence. It is interesting to note that, although reflection of light on the smooth surface of objects may sometime produce artifacts in the grayscale image, the application of image processing techniques is able to fill the holes in the image and loosen the problem. Although the mark on the cup sometimes appears as

a hole in binary image, the size is significantly reduced and can be compensated by active sensing (see below). As a result, all the three objects in the grayscale image were vividly transferred into downsampled binary image with little loss of shape information.

The records from both fixed and active cameras were analyzed by the trajectory tracking algorithm. Figure 6 demonstrates one of the results. The left column shows images acquired from the active camera. The middle column shows the most similar image blocks acquired by the fixed camera, as shown in the right column, which included images acquired from the fixed camera with the most similar regions marked. It can be seen that images acquired from active and fixed cameras differ in some sense because of distinct shot angles and orientations. However, the proposed trajectory tracking algorithm for the TVSS constantly succeeded in locating the most similar blocks from the fixed images.

After locating the image blocks from the fixed camera that is most similar to that from the active camera, the trajectory of the active camera movement could be tracked. Figure 7 shows one of the results. The red points in the figure show the center points of the located most similar images to the active images. The result shows that the participant moves her hand back and forth trying to identify objects in the scene according to the tactile stimuli generated from the device. In this case, the participant moved more frequently in the horizontal direction than in the vertical direction searching for objects. After she "felt" an object, she focused on the edges as an attempt to identify the objects. The trajectory tracking provides an insight into the participants' behavior and strategy in using the TVSS for exploring the surrounding environments.

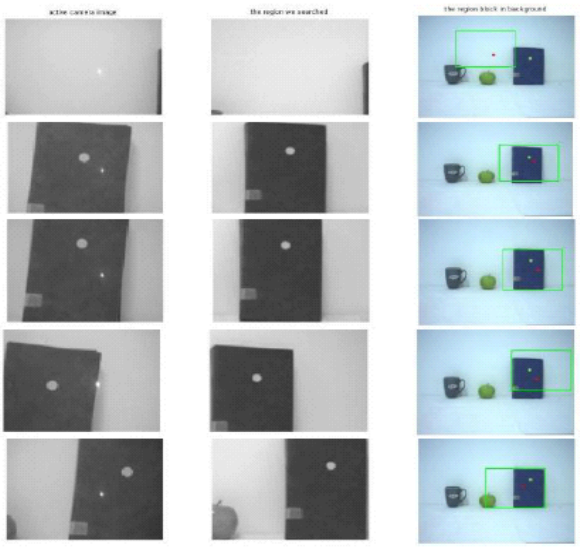

Figure 6. Results of TVSS trajectory algorithm; left: images from the active camera; middle: most similar image blocks in the fixed camera; right: images from the fixed camera with the marked most similar regions.

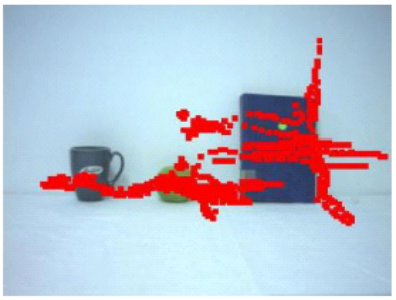

Figure 7. Trajectory of the active camera

VI. CONCLUSION

This paper presents the preliminary result of the Tactile Visual Substitution System developed for the study of active sensing. Two subsystems were developed. The image processing subsystem solves the problems, such as high-to-low resolution transformation, light reflection on the surface of objects, and texture artifacts, usually encountered by traditional TVSS. The trajectory tracking subsystem, on the other hand, enables the researchers to trace the movement of the tactile device which reflects the strategies employed by the TVSS user to explore the environment. The preliminary results of the study demonstrate the capability of the system in offering a more effective TVSS and a more powerful diagnosis system for the study of active sensing of the visually impaired.

ACKNOWLEDGMENT

This study was supported in part by the grant NSC 99-2923-E-194-002-MY2 from the National Science Council, Taiwan, a grant from the Ministry of Education, Taiwan, R.O.C. and the grant 710863 from the Ministry of Science and Technology, Israel.

REFERENCES

[1] E. Ahissar, M. Abeles, M. Ahissar, S. Haidarliu, and E. Vaadia, "Hebbian-like functional plasticity in the auditory cortex of the behaving monkey," *Neuropharmacology*, vol. 37, pp. 633-655, 1998.

[2] V. Ego-Stengel, D. E. Shulz, S. Haidarliu, R. Sosnik, and E. Ahissar, "Acetylcholine-dependent induction and expression of functional plasticity in the barrel cortex of the adult rat," *Journal of Neurophysiology*, vol. 86, pp. 422-437, 2001.

[3] P. Bach-y-Rita, C. C. Collons, F. A. Saunder, B. White, and L. Scandden, "Vsion Substitution by Tactile image projection," *Nature*, vol.221,, pp. 963-4, 1969.

[4] P. Bach-y-Rita and S. W. Kercel,"Sensory substitution and the human-machine interface," *Trends in Cognitive Neuroscience,* vol.7, no.12, pp.541-546, 2003.

[5] P. Bach-y-Rita and K. A. Kaczmarek, "Tongue placed tactile output device," *US Patent* 6,430, 450, 2002.

[6] L Renier and A. G. De Volder, "Cognitive and brain mechanisms insensory substitution of vision: a contribution to the study of human perception," *J Inter Neurosci* 4, pp. 489-503, 2005.

[7] http://www.tactile-world.com/.

[8] R. C. Gonzalez and R. E. Woods, Digital Image Processing, 3rd ed., New Jersey: Prentice Hall, 2007.

[9] S.-N. Yu, and C.-N. Lin, "An Efficient Paradigm for Wavelet-based Image Processing Using Cellular Neural Networks," *International Journal of Circuit Theory and Applications*, vol. 38, no. 5, pp. 527-542, June 2010.

[10] C.-N. Lin and S.-N. Yu, J.-C. Hu, "Image Processing for a Tactile /Vision Substitution System Using Digital CNN," *28th Annual International Conference of IEEE Engineering in Medicine and Biology Society*, Aug. 30-Sep. 3, 2006, New York, USA.

[11] http://homepages.inf.ed.ac.uk/rbf/HIPR2/morops.htm.

[12] A. Saig, G. Gordon, E. Assa, A. Arieli, E. Ahissar, "Motor-sensory confluence in tactile perception," *Journal of Neuroscience*, vol. 32, pp. 14022–14032, 2012.

A Portable Real-time ECG Recognition System Based on Smartphone*

Tzu-Hao Yen, Chung-Yu Chang, and Sung-Nien Yu, *Member, IEEE*

***Abstract*—This paper proposed an smartphone-based real-time ECG monitoring and recognition system. The ECG signal was acquired by a MSP430FG4618 low-power microprocessor and was converted via a Bluetooth module for wireless transmission to a smartphone. A noise-tolerant ECG heartbeat recognition algorithm based on discrete wavelet transform and higher-order statistics was employed to identify different types of heartbeats. This system achieved a high accuracy of 98.34 % in identifying seven heartbeat types, which was demonstrated to outperform other studies in the literature. The heartbeat types were recognized in real-time; only 78 ms was required to identify a heartbeat. The portability, real-time processing, and high recognition rate of the system demonstrate the efficiency and effectiveness of the device as a practical computer-aided diagnosis (CAD) system.**

I. INTRODUCTION

In recent years, the mortality of cardiovascular disease has always been on top of the list, thus effective diagnosis and treatment of these diseases has become a major issue in the hospital. The first step in diagnosing cardiovascular diseases usually depends on the recording and analysis of electrocardiogram (ECG), which measures the electrical activity of the cardiac conduction system. However, ECG measurement usually requires the patients to carry a device, e.g. a Holter, for more than 24 hours and record the signal. The recorded ECG signals are then brought back to the hospital to be examined by the physicians. This process would take a long period of time and some mistakes or ignorance of minor signs could be made. These issues give rise to the requisite of portable ECG recording and recognition system.

Portable ECG products are not common in the medical market. The reason is expensiveness. Therefore, if the terminal device could be replaced by consumer electronics that are possessed by a great portion of common people, the cost of the device can be extensively lowered. According to the publication of International Telecommunication Union in January 2011 [1], the global mobile phone users have exceeded 50 billion people. Moreover, the International Data market share has been as high as 39.5% in 2011 and expected that it will grow to 45% in 2015. The report indicates there will be more and more users have Android mobile devices.

Android is an open platform which enables the developer to take advantages of the many features provided by the platform to build novel applications. Several attempts have been made to develop portable ECG devices based on Android mobile devices. For example, the two companies Polar and Zephyr have developed an Android platform compatible Bluetooth heartbeat belt. The ECG signal and the calculated heart rate are transmitted to the Android phone by Bluetooth. However, previous research usually focused on ECG and heart rate monitoring, yet lack the capability of arrhythmia detection and diagnosis.

Therefore, we propose to integrate wireless ECG transmutation, heart rate monitoring, and real-time arrhythmia recognition in an Android smartphone. The objective was to build a convenient and effective portable computer-aided diagnosis (CAD) system.

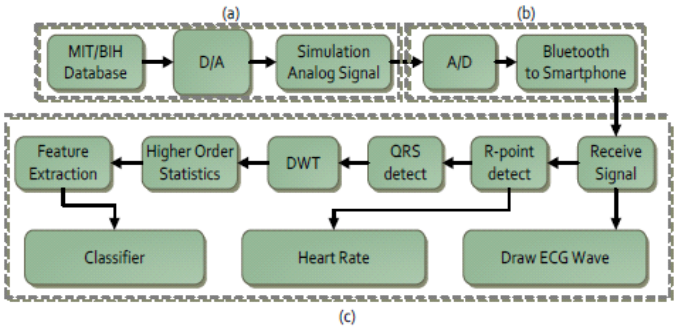

Figure 1. The architecture of the proposed system. (a) Generation of simulated ECG signals; (b) analog to digital conversion (A/D) and Bluetooth transmission; (c) ECG signal monitoring and processing with smartphone.

II. METHOD

The architecture of the proposed system is depicted in Fig. 1. This system is divided into three functional blocks, namely (a) generation of simulated ECG signals; (b) analog to digital conversion (A/D) and Bluetooth transmission; (c) ECG signal monitoring and processing with smartphone, each of which will be described separately in the following sections.

A. Generation of Simulated ECG Signals

A virtual instrument built with LabVIEW program and NI DAQmx input/output device was developed to generate simulated ECG signals for the experiments. The ECG signals were extracted from the MIT/BIH arrhythmia database. By programming an analog output with the data files and setting

*Research supported by the National Science Council and the Ministry of Education, Taiwan, Republic of China.

Tzu-Hao Yen and Chung-Yu Chang are with the Department of Electrical Engineering and the Advanced Institute of Manufacturing with High-tech Innovations, National Chung Cheng University, Chiayi County, Taiwan (e-mail: isverlis@gmail.com; taco.killua@msa.hinet.net).

Sung-Nien Yu is with the Department of Electrical Engineering and the Advanced Institute of Manufacturing with High-tech Innovations, National Chung Cheng University, Chiayi County, Taiwan (corresponding author's phone: +886-5-2720411 ext 33205; fax: +886-5-2720862; e-mail: ieesny@ccu.edu.tw).

the sampling rate as 360 Hz, simulated ECG signals based on the real data were generated for testing the performance of the system.

B. Analog to Digital Conversion (A/D) and Bluetooth Transmission

A microcontroller MSP430FG4618 (Texas Instruments Co., Ltd., America) was selected to convert the analog signal to digital [7]. The MSP430 family is designed for low cost, low power consumption embedded applications, which is particularly well suited for developing battery-powered portable device. The controller provides 12-bit A/D converters that would be sufficient for ECG signal acquisition. Since MSP430FG4618 only accepts voltage ranging between 0 V and 2.5 V, signals were boosted by +1.5V using LM358-OP (Texas Instruments Co., Ltd., America) to avoid possible aliasing or saturation.

The HC-05 chip (Wavesen Co., Ltd., China) was used to convert the RS232 serial output from MSP430FG4618 to Bluetooth 2.0 format. HC-05 is characterized as convenient, low-power, and low-cost [3]. It replaced RS232 to communication wirelessly between the MSP430FG4618 and the smartphone.

D. R-point Detection

A median filter with appropriate window size was firstly used eliminate the baseline wander in the ECG signal. Then, the Pan and Tompkins algorithm [4] was used to locate the R points of the heartbeats. Once the R points were located, 64-point QRS segments centered at R point were extracted from the record for the calculation of features for each heartbeats.

E. Feature Calculation

The feature sets play a major role in the effectiveness of a classifier. We have previously applied higher-order statistics (or cumulant) and simple RR-interval features to characterize ECG signals for heartbeat type recognition and successfully implemented a noise-tolerant ECG classifier on a desk-top computer [5]. The application of higher order statistics for characterizing signals has been shown to be effective in suppressing the influence of a wide range of noises and artifacts [5]. In this study, we adopted the same ideas with minor modification and intended to fulfill the classifier on a smartphone with Android platform. The challenges would be the high speed requirement of a real-time system and the much lower computational speed of the smartphone when compared to a desk-top computer.

With each R point in the ECG signal, a 64-point QRS segment centered at the R point was extracted. A five-level DWT was used to decompose the segment into different subband components. Higher-order (2^{nd}, 3^{rd}, and 4^{th}) cumulants were calculated based on the components. For clarity, the j^{th} order cumulant of the D_i subband was denoted as C_{ij} where $i \in \{3, 4, 5\}$ and $j \in \{2, 3, 4\}$. Four sets of cumulant-related features and three RR interval-related features were recruited in this study [6][11]. These features are explained separately as follows.

1. Standard Deviation of the Cumulant (CSD): the standard deviation of the cumulant is defined as:

$$\sigma_{ij} = \sqrt{\frac{1}{2L}\sum_{l=-L}^{L}[c_{ij}(l) - \overline{c_{ij}}]^2} \qquad (1)$$

   $i \in \{3, 4, 5\}$ and $j \in \{2, 3, 4\}$, where $\bar{c}_{ij}$ is the sample mean of the cumulant and l is the time shift ranging from –L to +L.

2. Normalized Summation (NS): the normalized summation is defined as the sum of cumulants divides the sum of the absolute cumulant, such that $i \in \{3, 4, 5\}$ and $j \in \{2, 3, 4\}$.

$$NS_{ij} = \sum_{l=-L}^{L} c_{ij}(l) \Big/ \sum_{l=-L}^{L} \left| c_{ij}(l) \right| \qquad (2)$$

3. Number of Zero-Crossings (NZC): The number of zero-crossing is important in characterizing the variation of a signal. Since the D_5 subband was observed to show distinct zero-crossing features among different beat types, we focused on the three higher-order cumulants of D_5, i.e. C_{52}, C_{53}, and C_{54}.

4. Symmetry (SYM): The.symmetry is defined as:

$$SYM_{ij} = \sum_{l=1}^{L} \left| c_{ij}(l) - c_{ij}(-l) \right| \Big/ \sum_{l=-L}^{L} \left| c_{ij}(l) \right| \qquad (3)$$

   $i \in \{3, 4, 5\}$ and $j \in \{3, 4\}$. Since the Symmetry of the 2^{nd} cumulant is zero, we only need to extract from the 3^{rd} and 4^{th} cumulants.

5. RR Interval-related Features: The RR interval is defined as difference in the time between two adjacent R peaks. We extracted three RR interval-related features, including the instantaneous RR interval, the ratio between the instantaneous and the previous ones, and the ratio between the previous and the one before it.

In summary, the feature vector contains 30 features, including nine CSDs, nine NSs, three NZCs, six SYMs, and three RR interval-related features. Each feature was normalized by subtracting the mean value from the feature and dividing by the feature's standard deviation. This process intended to normalize all the features to the same level.

F. Classification

The back propagation neural network (BPNN) is a multi-layer perceptron (MLP) [8] which has been proven to be suitable for use in the classification of nonlinear data. The typical BPNN consists of three layers, including an input layer, a hidden layer, and an output layer. Hyperbolic tangent sigmoid function is used as activation function and the weights between neurons of consecutive layers are modified by back propagating the error signals backwardly layer by layer to approach optimal solution. The number of neurons in the hidden layer would affect the nonlinearity of the neural classifier, and is empirically chosen as sixty. The training phase of the classifier was done on a desk-top computer and the optimal weights were saved and downloaded onto the

smartphone for the classifier in the testing phase of the real-time classifier.

G. Android Platform

There are two reasons for choosing Android platform in the study. First, Android is an open source platform that based on the Java of Linux core system and the Android SDK provides the tools and APIs necessary to begin developing applications on the Android platform. Second, Android smartphone has successfully gained a significant market share in recent years. In this study, we used HTC Incredible S. The phone has CPU 1GHz, 768MB RAM and runs the version 2.3.2 of Android operational system [9].

The flow chart of the functions on the smartphone is depicted in Fig. 2. First of all, the Bluetooth function on the smartphone must be turn on, which then searches for the nearby device for connection. Once connected, the smartphone begins to receive the raw ECG data transmitted from the HC-05 chip and display on the screen. The received data was processed in a five-second basis. The R points were first located and the feature sets and heart rates were calculated. The features were fed into the trained BPNN classifier and the results were displayed on the screen. The raw data, heart rate, and ECG type were saved to the SD card.

III. Results and Discussions

The first step in using this system was connecting the smartphone to the Bluetooth data transmission. A Bluetooth connecting interface was developed. After touching the button on the smartphone, three functional keys appear on the screen (Fig. 3 (a)). Touching the "Make discoverable" key enables the smartphone to search for nearby Bluetooth devices. After touching the "Connect a device" key, the names of these devices are shown on the screen (Fig. 3 (b)). Select a device and the smartphone would try to connect to it through Bluetooth. If Bluetooth is connected successfully, the received ECG data are shown on the screen. If the connection failed, the system would show an alarm sign of "Not connected and request for another connection.

The graphic user interface (GUI) includes the display of ECG waveform, heart rate, and recognized beat type, as depicted in Fig. 4. The heart rate was calculated from the inverse of the averaged five consecutive RR-intervals, intending to reduce the heart rate errors caused by false detection of R peaks. The waveform was displayed and processed in a 5-sec basis and the average time to classify a beat type was 78 ms.

To evaluate the performance of the system in ECG recognition, fifteen records (100, 105, 106, 109, 111, 114, 116, 118, 119, 124, 200, 207,209, 212, 214) were selected from the MIT / BIH arrhythmia database [10]. The performance of the system was measured by the recognition rates of individual beat types and the average accuracy.

With the analog ECG signals simulated by the virtual instrument built with LabVIEW program and NI DAQmx input/output device, the recognition rates of the portable real-time ECG beat recognition system were calculated and summarized in Table I. An impressively high average

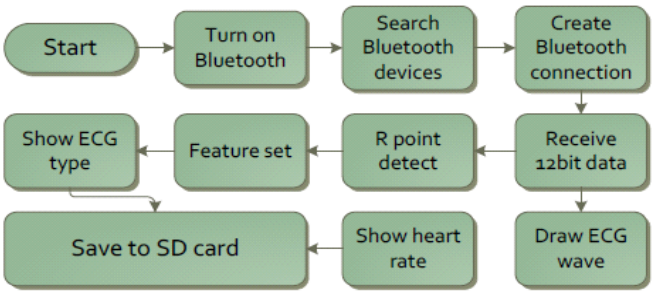

Figure 2. Flow chart of the programs on the smartphone.

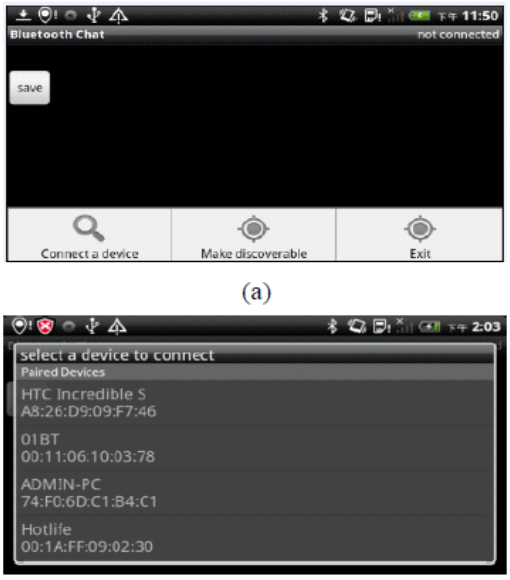

Figure 3. (a) Bluetooth make discoverable and (b)connect a device process.

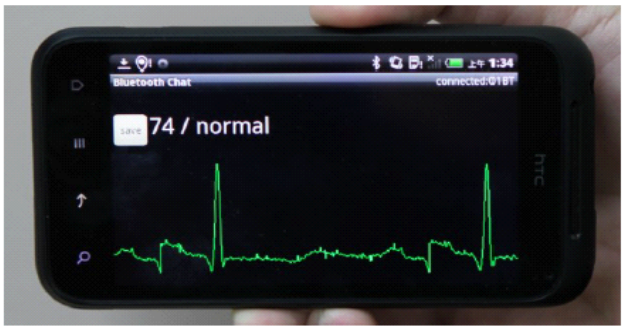

Figure 4. Graphic user interface on the smartphone.

TABLE I. Classification results using BPNN

ECG beat type	*Recognition rate (%)*
NORMAL	98.98
LBBB	98.58
RBBB	97.62
PVC	97.70
APB	88.29
VEB	93.27
VFW	92.68
Average accuracy	98.34

accuracy of 98.34 % was achieved. It is noticeable that the recognition rates were high across different beat types. The lowest rate of 88.29 % was associated with Atrial premature Beats (APB). Referring to our other studies [11], the recognition rates of APB were usually among the lowest. The requirement of real-time and accurately detecting the R-points for calculating effective features further deteriorated the results. This may be improved by modifying the R-point detection algorithm and adding more APB samples in the training phase of the classifier.

It is also interesting to compare the performance of the proposed method to that of other studies. Three effective methods [12-14] were selected for comparison. The comparative results are summarized in Table II. The high average accuracy of the proposed method outperforms the other three methods in discriminating the highest number (seven) of beat types when compared to five in [13] and four in [14]. The results in Tables 1 and 2 support the effectiveness of using the proposed method in a smartphone to discriminate ECG arrhythmias in real-time.

The quick classification and high accuracy of the system demonstrated the feasibility of the system as an effective portable and real-time device for ECG beat recognition.

IV. CONCLUSION AND FUTURE WORK

A portable and real-time cardiac arrhythmia recognition system based on smart phone was proposed in the study. The ECG signal was acquired by a MSP430FG4618 controller and transmitted wirelessly through Bluetooth by a HC-05 chip. The signal was received and processed on a smart phone with Android platform. A noise-tolerant algorithm based on wavelet decomposition and higher-order statistics were exploited to identify the heartbeat types. This method was demonstrated to be effective and efficient. High accuracy of 98.34 % was achieved to successfully differentiate seven types of heartbeats with a short average recognition time of 78 ms/beat. The proposed system was demonstrated to outperform other systems published in the literature. The portability and real-time processing capabilities of the system further enhance the clinical value of the system as a computer-aided diagnosis (CAD) device.

This paper shows the prototype of the system. However, this prototype still leaves room for improvement, such as refining the graphic user interface and improving the recognition rate of APB. Furthermore, other physiological parameters, such as temperature, blood pressure, blood oxygen level, etc., could be integrated to build a portable multi-functional health monitoring device with real-time computer-aided diagnosis.

ACKNOWLEDGMENT

This study was supported in part by the grants NSC 100-2221-E-194-063 and NSC101-2221-E-194-019 from the National Science Council and a grant from the Ministry of Education, Taiwan, Republic of China.

TABLE II. Comparison of different ECG beat classification methods.

Method	*Number of beat type*	*Accuracy*
FHyb-HOSA [12]	7	96.06 %
MME [13]	5	97.78 %
Neuro-Fuzy [14]	4	98.00 %
This Study	7	98.34 %

REFERENCES

[1] International Telecommunication Union http://www.itu.int/zh/Pages/default.aspx

[2] International Data Corporation (IDC) http://www.idc.com.tw/

[3] S.-Y. Ko, K.-M. Wang, W.-C. Lian, and C.-H. Kao, "A portable ECG recorder," 2012 2nd International Conference on Consumer Electronics, Communications and Networks (CECNet), 2012, pp. 3063-3067.

[4] J. Pan and W. J. Tompkins, "A real-time QRS detection algorithm," IEEE Transactions on Biomedical Engineering, vol. 32, pp. 230-236, 1985.

[5] J. Jakubowski, K. Kwiatos, A. Chwaleba, and S. Osowski, "Higher order statistics and neural network for tremor recognition," IEEE Transactions on Biomedical Engineering, vol. 49, pp. 152-159, 2002.

[6] Y.-H. Chen and S.-N. Yu, "Subband features based on higher order statistics for ECG beat classification," 29th Annual International Conference of the IEEE Engineering in Medicine and Biology Society (EMBC), 2007, pp. 1859-1862.

[7] L. Wei, H. Sheng, S. Zhenzhou, and T. Jindong, "A real-time cardiac arrhythmia classification system with wearable electrocardiogram," 2011 IEEE International Conference on in Cyber Technology in Automation, Control, and Intelligent Systems (CYBER), 2011, pp. 102-106.

[8] F. A. Varella, G. L. de Lima, C. Iochpe, and V. Roesler, "A method for the automatic classification of ECG beat on mobile phones," 2011 24th International Symposium on Computer-Based Medical Systems (CBMS), 2011, pp. 1-6.

[9] S. Gradl, P. Kugler, C. Lohmuller, and B. Eskofier, "Real-time ECG monitoring and arrhythmia detection using Android-based mobile devices," in Engineering in Medicine and Biology Society (EMBC), 2012 Annual International Conference of the IEEE, 2012, pp. 2452-2455.

[10] MIT-BIH Arrhythmia Database(mitdb) http://www.physionet.org/cgi-bin/atm/ATM

[11] S. N. Yu and Y. H. Chen, "Noise-tolerant electrocardiogram beat classification based on higher order statistics of subband components," Artif Intell Med, vol. 46, pp. 165-78, Jun 2009.

[12] S. Osowski and L. Tran Hoai, "ECG beat recognition using fuzzy hybrid neural network," IEEE Transactions on Biomedical Engineering, vol. 48, pp. 1265-1271, 2001.

[13] M. Engin, "ECG beat classification using neuro-fuzzy network," Pattern Recognition Letters, vol. 25, pp. 1715-1722, 2004.

[14] İ. Güler and E. D. Übeyli, "A modified mixture of experts network structure for ECG beats classification with diverse features," Engineering Applications of Artificial Intelligence, vol. 18, pp. 845-856, 2005.

Detection of Myocardial Ischemia Episode Using Morphological Features*

Cheng-Hsiang Fan, Yu Hsu, Sung-Nien Yu, *Member, IEEE*, and Jou-Wei Lin

***Abstract*—In this study, we propose to use morphological features that are easy to identify to differentiate myocardial ischemic beats from normal beats. In general, myocardial ischemia causes alterations in electrocardiographic (ECG) signal such as deviation in the ST segment. When the ST segment level deviates from a certain voltage, the beat would be diagnosing as myocardial ischemia. To emphasize on ST variations, the QRS complex of the ECG signal was first subtracted and replaced with a straight line. Five–level discrete wavelet transform (DWT) followed to decompose the waveform into subband components and the A5 subband, which is most sensitive to the changes in the ST segment, was reconstructed for the calculation of 12 morphological features. The support vector machine (SVM) and the 10-fold cross-validation method were employed to evaluate the performance of the method. The results show high values of 95.20%, 93.29%, and, 93.63% in sensitivity, specificity, and accuracy, respectively, that were demonstrated to outperform the other methods in the literature.**

I. INTRODUCTION

"Myocardial ischemia is the pathological state underlying ischaemic heart disease. It can lead to myocardial infarction (commonly known as heart attack) which in its acute form can lead to the death of the affected person." [1]. The most important cause of myocardial ischemia is coronary artery stenosis or obstruction. Myocardial ischemia causes alterations in electrocardiographic (ECG) signal such as deviation in the ST segment [2]. When the ST segment deviates more than a certain level, the beat would be diagnosing as myocardial ischemia.

Recently, several studies have been conducted to developing computer-aided diagnosis algorithms for the diagnosis of myocardial ischemia. Exarchos and coworkers proposed to use rule-based mining technology to identify myocardial ischemia heartbeat from normal heartbeat in 2006 [3]. Khoshnoud and coworkers used subband ECG signal decomposition with multi-level wavelet analysis and claimed that their method provided an easier way to locate the important points of the waveform for myocardial ischemia diagnosis with probabilistic neural network (PNN) [4].

*Research supported by the National Science Council and the Ministry of Education, Taiwan, Republic of China.

Cheng-Hsiang Fan, Yu Hsu, and Sung-Nien Yu are with the Department of Electrical Engineering and the Advanced Institute of Manufacturing with High-tech Innovations, National Chung Cheng University, Chiayi County, Taiwan (phone: +886-5-2720411 ext 33205; fax: +886-5-2720862; e-mail: fanchenshan@gmail.com; anderson23i@hotmail.com; ieesny@ccu.edu.tw (corresponding author)).

Jou-Wei Lin is with the Cardiovascular Center, National Taiwan University Hospital Yun-Lin Branch and the College of Medicine, National Taiwan University, Dou-Liou City, Yun-Lin County, Taiwan. (e-mail: jouweilin@yahoo.com).

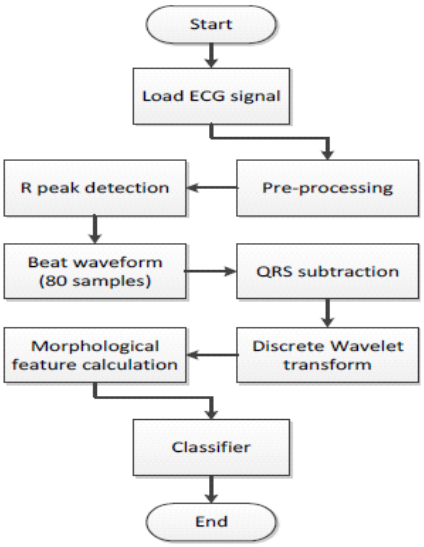

Figure 1. Experimental procedure.

However, conventional methods usually required to find the fiducial points, e.g. T wave, R peak, ISO point, J point, as features for myocardial ischemia detection [5], but the fiducial points may not be easy to locate when the ECG signal is noisy. Therefore, in this study, we proposed to use morphological features that were calculated from the entire heartbeat waveform. With this method, only the R point of the heartbeat, which is the easiest to locate, is to be located and the requisite of extremely clean signal for accurately locating several key points is loosened. The performance of the method was validated using support vector machine classifier and 10-fold cross-validation method.

II. METHODS

A. Database:

The data used in the experiments were obtained from the "European Society of Cardiology (ESC) ST-T database" [6]. This database includes 78 data files recorded from myocardial ischemia patients. Each file contains two-lead, two-hours ECG signals sampled at 250 Hz. The start and end times of the ST-segment changes (myocardial ischemia episode; MI episode) were clearly annotated in the files.

B. Discrete Wavelet Transform

Discrete wavelet transform (DWT) was employed to decompose the ECG signals into subband components. The DWT provides a good time-frequency representation of a signal by using variable sized windows. Long time windows

are used to get a finer low frequency resolution. Short time windows are used to get high frequency information. WT is suitable for the analysis of non-stationary signals such as ECG.

The ECG signal can be decomposed into finer details by multi-level discrete wavelet transform (DWT) using high-pass (*g[n]*) filter, low-pass (*h[n]*) filter, and downsampling (↓2). [7]. After the first level decomposition, two signals representing the detail (high-frequency) and the approximate (low-frequency) are obtained. The approximate signals are further decomposed into the detail and the approximate after the second level decomposition, et al, as depicted in Fig. 2 (a). Subband components can be reconstructed back to the length of the original signal *x[n]* by inverse DWT (IDWT), as depicted in Fig. 2 (b). This process can also be used to eliminate noises by setting components in certain subbands to be zero and perform the IDWT.

C. Preprocessing

The aim of the preprocessor was to remove the baseline wander and noise artifacts frequently observed in ECG signals. ECG baseline wander usually caused by breathing or unexpected movement of experimental settings, which usually cover the frequency range below 1Hz [8]. In order to eliminate baseline wander, we used DWT to decompose signal to the seventh level and then set the approximate coefficient A7 to zero and perform the IDWT. In this manner, subband components below 0.97 Hz were removed from the signal.

The second part of the preprocessor was to remove noise artifacts.The soft-thresholding method proposed by Donoho [9] was adopted for this purpose. Seven levels of DWT were applied to the signal first. The subband coefficients with minor values were considered noise and were set to zero before the application of IDWT to eliminate the noise.

D. R Peak Detection

In order to accurately locate the R peaks in ECG, we focused only on the D_3 and D_4 subband components that show the most significant features of the QRS complex [10]. First of all, all the other subband components, except that of D_3 and D_4, were set to zero. Moreover, to highlight the location of the QRS complex, the coefficient values in both D_3 and D_4 were squared and the smaller values (threhold= standard deviation of the reconstruction signal) eliminated before performing IDWT. The location of the peaks in the reconstructed signal were the tentative positions of the R peaks, as depicted in Fig. 3 (a). However, since DWT sometimes causes minor shift of the waveform, the positions of the real R peaks (Fig. 3 (b)) were determined by searching the highest peaks in the vicinity (±10 samples) of the tentative R peaks (Fig. 3 (a)) in the preprocessed ECG signal.

E. Calculation of Morphological Features

After the R peak has been located, a 80-point waveform, with 35 samples before and 44 samples after the R peak (Fig. 4), was segmented as the representative waveform of a

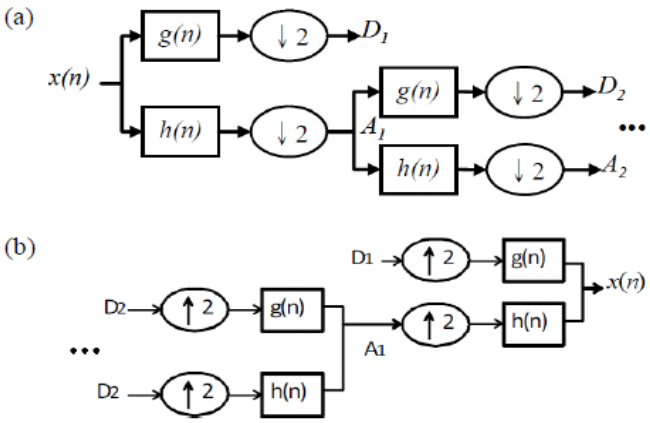

Figure 2. Discrete wavelet transform (DWT). (a) forward DWT (decomposition); (b) inverse DWT (reconstruction).

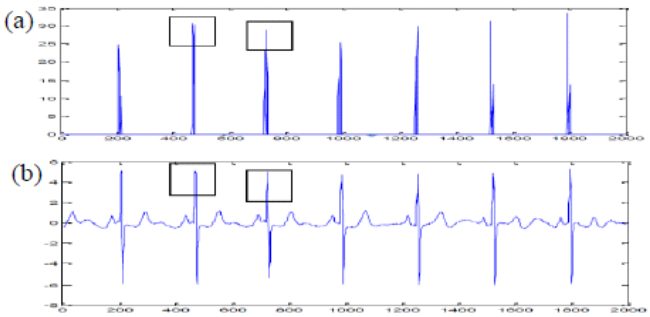

Figure 3. R peak detection. (a) tentative R peaks; (b) real R peaks after vicinity searching.

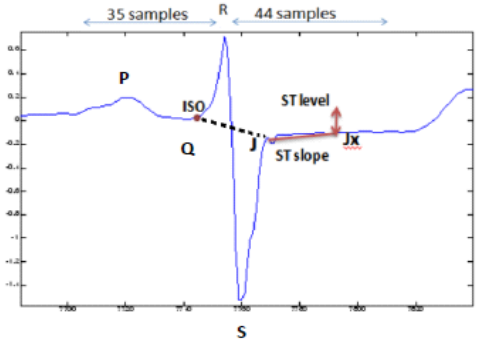

Figure 4. 80-sample ECG waveform of a heartbeat.

heartbeat. The three points *J*, *JX*, and *ISO* closely related to the R peak were first located on the waveform according to the heart rate, as shown in Table I and Fig. 4. The QRS complex was defined as the part of waveform between the *ISO* and *J* points. In order to concentrate only on the features associated with ST segment, the QRS complex was first removed from the original waveform and replaced with a straight line (dash line in Fig. 4).A five-level DWT followed to decompose the QRS subtracted waveform into different subbands. The low-frequency part (A5) of the 5th-level DWT was reconstructed using IDWT. Six features were exploited to characterize the reconstructed A5 component, namely (1) the power the A5 component (Power), (2) the power ratio of the A5 to the original signal (Power ratio), (3) JX potential, (4) ST

level, (5) ST deviation, and (6) ST slope, as summarized in Table II.

In order to characterize the variation of the waveform from a typically "normal" one, a reference waveform was generated by calculating the average waveform of the 80-point beat waveforms in the first 30 sec record, as adopted by the European Society of Cardiology to calculate the "normal" waveform for the database [6]. Six features associated with the relationship between the reconstructed A5 components from the test and the reference waveforms were calculated, including (1) the correlation coefficient (CC), (2) the mean (Mean_CF) and (3) the standard deviation (SD_CF) of the cross-correlation function, and (4) the mean (Mean_D), (5) the standard deviation (SD_D), and (6) the power (Power_D) of the difference waveform between the test and reference waveforms.

Each feature was normalized by subtracting the mean value from the feature and dividing by the feature's standard deviation. This process intended to normalize all the features to the same level.

F. Support Vector Machine Classifier

Support vector machine (SVM) maps the training samples from the input space into a higher-dimensional feature space via a mapping (kernel) function [11]. Any product between vectors in the optimization process can be implicitly computed to generate a hyperplan to categorize the samples into two classes.

For a training set of instance-label pairs (x_i,y_i), i=0,…l, where $x_i \in R$ and y_i=[-1,1], and a non-linear operator mapping with kernel function φ, the optimization problem becomes

$$\min_{w,b,\xi} \frac{1}{2} w^T w + S\sum_{i=1}^{l} \xi_i \qquad (1)$$

$$\text{subject to} \quad y_i(w^T \varphi(x_i) + b) + \xi_i - 1 \geq 0, \xi_i \geq 0$$

where $S>0$ is the penalty parameter for the error term and ξ_i is the set of slack variables that is introduced when the training data is not completely separated by a hyperplane. To solve this problem, Vapink [11] has shown that the solution can be found by minimizing both the errors on the training set (empirical risk) and the complexity of the hypothesis space. Consequently, the decision found by SVM is a tradeoff between error and model complexity. Numerous studies have demonstrated the superiority of using SVM classifier over other classifiers in pattern classification tasks. Consequently, we employ the SVM classifier in the study. The radial basis function (RBF) was empirically selected as the kernel function of the SVM classifier.

III. RESULTS AND DISCUSSIONS

Fourteen data files were selected from the database for experiments. Based on the information about myocardial ischemia episode provided by the database, 3970 ischemic and 28890 normal heartbeat waveforms were segmented from the data files for analysis.

TABLE I. LOCATIONS OF THE KEY POINTS

Heart rate (HR)	*J*	*JX*	*ISO*
HR > 120 bpm	R+40ms	R+60ms	R-40ms
120 bpm > HR > 100 bpm	R+40ms	R+60ms	R-40ms
HR < 120 bpm	R+60ms	R+80ms	R-40ms

TABLE II. MORPHOLOGICAL FEATURES CALCULATED FROM THE QRS REMOVED WAVEFORM

Feature	***Feature Description***	
Power	Power of the A5 subband signal	Feature 1
Power ratio	Power ratio of the A5 subband to the original signal	Feature 2
JX potential	Potential of the *JX* point	Feature 3
ST level	Potential difference between *J* and *ISO*	Feature 4
ST deviation	ST level change from the normal	Feature 5
ST slope	Slope of the segment between *J* and *JX*	Feature 6
CC	Correlation coefficient of the test and reference waveforms	Feature 7
Mean_CF	mean of the cross-correlation function	Feature 8
SD_CF	Standard deviation of the cross-correlation function	Feature 9
Mean_D	Mean of the difference waveform of the test and reference waveforms.	Feature 10
SD_D	Standard deviation of the difference waveform	Feature 11
Power_D	Power of the difference waveform	Feature 12

The performance of the classifier was measured by three statistics indices, namely (1) specificity: the percentage of correctly classified normal beats among the total normal beats; (2) sensitivity: the percentage of correctly classified myocardial ischemia beats among the total ischemic beats; (3) accuracy: the percentage of correctly classified beats among all the beats.

The ten-fold cross-validation method [12] was employed to evaluate the performance of a classifier. The test sample beats were firstly divided into ten test sample groups with the same distribution of attribute. Each sample group was alternatively reserved as the test group. The other nine groups were used to train the classifier and the performance of the classifier was measured by using the reserved group as test samples. This procedure repeats until all the sample groups had been reserved once as test samples. The performance of the classifier was evaluated by the average values of the three indices in the ten trials.

The results were summarized in Table III. The proposed morphological features and SVM classifier achieved a sensitivity of 84.69% and a specificity of 97.25%, resulting in

an accuracy of 95.22%. The results were impressive, especially with the high specificity and accuracy. However, we have noticed that the sensitivity was much lower than the specificity. This phenomenon was caused by the imbalanced data sets, which would favor the major (normal) class and ignore the minor (ischemic) class.

Therefore, we sought to resolve this problem with over-sampling [13], which increases the number of samples in the minor class with data interpolation (or over-sampling) based on the real samples to the same level of the major class. The performance of the classifier using over-sampling in the training phase is demonstrated in Table IV. Comparing the performance in Table III and Table IV, a dramatic increase in the sensitivity was observed with the over-sampling technique. Only a minor decrease in specificity was observed, which was believed to be the compensation caused by oversampling in the minor (ischemic) class. The two effects resulted in a classifier equally effective in recognizing normal and ischemic ECG beats.

The performance of the proposed system was compared to that of two representative methods published in the literature, although the databases were not exactly the same. One is the rule-based mining method proposed by Exarchos and coworkers [3], which achieved 87% in sensitivity and 93% in specificity. The other is the method proposed by Khoshnoud and coworkers, who used subband ECG signals for locating important myocardial ischemic points for classification with probabilistic neural network (PNN) [4]. A sensitivity of 96.67% and a specificity of 89.18% were reported. The comparative results were summarized in Table V. It is impressive that the proposed method with over-sampling achieved sensitivity and high specificity, which is superior to the other methods that only show large value in either sensitivity or specificity. This property of the method is believed to be favorable for a computer-aided myocardial ischemia diagnosis system.

IV. CONCLUSION

We proposed a method for the detection of ischemic heartbeats based on morphological features. The objective of the study was to use only the R point which is easily identifiable and bypass the need to identify the key points that are apt to be buried in noise and might be difficult to be correctly located, such as the S and T points. Easily identifiable key points only depending on the location of the R point and the heart rate were used instead (Table I). Morphological features were calculated from the A5 subband components of the QRS complex subtracted waveform. This approach minimized the interference of the QRS complex in the calculation of ST-related features and only focused on the variation of the ST segment in characterizing ischemic waveform.

Impressive performance was observed with the morphological features. The application of oversampling technique to balance the samples in the two data sets further improved the performance of the classifier. The results demonstrate the effectiveness of the proposed method in accurately detecting ischemic beats using morphological features that are easy to calculate.

TABLE III EXPERIMENTAL RESULTS

Beat Type	Number of Samples (Train+Test)	Sensitivity (%)	Specificity (%)	Accuracy (%)
Ischemic	6489+722	84.69	97.25	95.22
Normal	33724+3748			

TABLE IV THE EFFECT OF OVER-SAMPLING IN ISCHEMIC CLASS

Beat Type	Number of Samples (Train+Test)	Sensitivity (%)	Specificity (%)	Accuracy (%)
Ischemic	33724+722	95.40	93.29	93.63
Normal	33724+3748			

TABLE V COMPARISON WITH OTHER STUDIES

Method	Sensitivity	Specificity	Accuracy
Rule-based [3]	87%	93%	90%
PNN classifier [4]	96.67%	89.19%	90.75%
Proposed method	95.40	93.29	93.63

ACKNOWLEDGMENT

This study was supported in part by the grants NSC 100-2221-E-194-063 and NSC101-2221-E-194-019 from the National Science Council and a grant from the Ministry of Education, Taiwan, Republic of China.

REFERENCES

[1] Wikipedia: Myocardial Ischemia http://en.wikipedia.org/wiki/Myocardial_ischemia

[2] M. S. Thaler, *The Only EKG Book You'll Ever Need*, 6th ed. New York: Lippincott Williams and Wilkins, 2009.

[3] T. P. Exarchos, C. Papaloukas, D. I. Fotiadis, and L. K. Michalis, "An association rule mining-based methodology for automated detection of ischemic ECG beats," *IEEE Trans. Biomed. Eng.*, vol. 53, no. 8, Aug. 2006.

[4] S. Khoshnoud, T. Mohammad, and M. A. Shoorehdeli, "Probabilistic neural network oriented classification methodology for ischemic beat detection using multi resolution wavelet analysis," *Proc. of the 17th Iranian Conference of Biomedical Engineering (ICBME2010)*, pp.1-4, 2010.

[5] K. Daskalov, I. A. Dotsinsky, and I. I. Christov, "Developments in ECG acquisition, preprocessing, parameter measurement, and recording," *IEEE Eng. Med. Biol.*, vol. 17, no. 2, pp. 50–58, Mar./Apr. 1998.

[6] European Society of Cardiology (ESC) ST-T Database: http://physionet.org/physiobank/database/edb/

[7] M. Weeks, *Digital Signal Processing Using MATLAB and Wavelets, 2nd ed.* Sudbury, MA: Jones and Bartlett Publishers, 2011.

[8] Z. Donghui, "Wavelet approach for ECG baseline wander correction and noise reduction," *27th Annual International Conference of the IEEE Engineering in Medicine and Biology Soiciety*, Shanghai, China, pp. 1212 - 1215, 2005.

[9] D. L. Donoho, "De-noising by soft-thresholding," *IEEE Trans. Information Theory*, vol. 41, no. 3, May, 1995.

[10] Z. Dabanloo, "Detection of QRS complexes in the ECG signal using multiresolution wavelet and thresholding method," *Computing in Cardiology*, pp. 805 - 808, 2011.

[11] V. N. Vapnik, *The Nature of Statistical Learning Theory*. New York: Springer-Verlag, 1995.

[12] R. M. Rangayyan, *Biomedical Signal Analysis: A Case-Study Approach*. New Jersey: John Wiley & Sons, 2002.

[13] H. Haibo and E. A. Garcia, "Learning from imbalanced data," *IEEE Trans. Knowledge and Data Eng.*, vol. 21, pp. 1263-1284, 2009.